



Evaluation of thermal and geometric properties of martensitic stainless steel thin walls built by additive manufacturing cold metal transfer (CMT) processes

Daniel Galeazzi¹ · Régis Henrique Gonçalves e Silva¹ · Alberto Bonamigo Viviani¹ · Pedro Rocha Jaeger¹ · Mateus Barancelli Schwedersky¹

Received: 12 October 2021 / Accepted: 11 February 2022 / Published online: 19 February 2022
© The Author(s), under exclusive licence to Springer-Verlag London Ltd., part of Springer Nature 2022

Abstract

Additive manufacturing is often seen as a novel alternative compared to well-consolidated, subtractive, and formative manufacturing processes. Its presence in the industrial environment is rapidly increasing, and its performance and flexibility may be the answer for present-day fabrication challenges, combining solutions to minimize environmental impacts without losing competitiveness or product quality. Arc welding-based additive manufacturing (also known as wire arc additive manufacturing, WAAM) has been gaining prominence in the current Industry 4.0 scenario. For the advancement of this technology, multiple output analysis of the pertinent welding processes is essential, especially regarding studies applied to materials such as high-strength and high-cost steels. In this paper, a study was conducted with the AISI 420 alloy and CMT variants of the GMAW process applied to additive manufacturing of thin walls, comparing them with conventional GMAW process. The welding processes and deposited welds used were analyzed on electrical, thermal, morphological, and metallurgical aspects. In the end, CMT Advanced and CMT Pulse variants stood out as opposite extremes, whereby CMT Advanced presented the best performance in relation to wall height and heat input. CMT and conventional GMAW produced good and significantly similar results, highlighting the stability of CMT.

Keywords Rapid prototyping · MIG/MAG · GMAW · Advanced welding processes · Welding 4.0 · Metal 3D print

Abbreviations

AM	Additive manufacturing
AISI	American Iron and Steel Institute
ASTM	American Society for Testing and Materials
BTF	Buy-to-fly
CG	Coarse-grain
CMT	Cold metal transfer
CTWD	Contact tip to work distance
DF	Dynamic feeding
GMAW	Gas metal arc welding
GTAW	Gas tungsten arc welding
HAZ	Heat affected zone
HSLA	High strength low alloy

HV	Hardness Vickers
PAW	Plasma arc welding
WAAM	Wire and arc additive manufacturing

1 Introduction

The additive manufacturing (AM) process is an emerging manufacturing technique in which a part is obtained through the sequential deposition of material layers [1, 2]. The additive manufacturing processes assisted by welding techniques are, according to Wu et al. [3], broadly classified into two categories: techniques that use high-power density welding processes (LASER and electron beam) and arc welding processes (PAW, GTAW, and GMAW), usually designated as WAAM, when the feedstock is in form of wire. Theoretically, the former allows producing parts in their geometry with the final tolerances; the latter currently allow producing components in semifinished state, called near-net shape [4].

✉ Daniel Galeazzi
daniel.galeazzi@posgrad.ufsc.br

¹ Mechanical Engineering Department, UFSC, LABSOLDA
— Welding and Mechatronics Institute, Florianópolis,
Santa Catarina, Brazil

The WAAM technique, as the name suggests, uses the electric arc as a heat source to perform additive manufacturing by directing it to a feedstock in form of wire, while it follows a deposition path. Williams et al. [5], Ding et al. [6], Cunningham et al. [7], and Horgar et al. [8] describe that the use of WAAM has been spreading industrially, especially in the aerospace sector, due to the advantages that the process offers. Main features to mention are reduction of the overall production time of the parts, quality obtained, and the possibility of manufacturing large and complex parts that by traditional methods could not be processed, including with noble materials. Another factor considered in the manufacturing of parts by the additive manufacturing process is the BTF factor. This term, originally from the aerospace industry, establishes the ratio between the initial volume of raw material and the final volume of the finished product. In this context, the main advantage of additive manufacturing processes lies in the fact that they present BTF factor equal or close to 1, much lower than conventional manufacturing processes (subtractive) that present average values of up to 11 as shown by Barnes et al. [9].

In conventional manufacturing, an initial blank structure is machined or conformed to obtain the final shape and tolerances of the desired part. This processing step will cause exacerbated material and energy waste depending on the shape and complexity of the final part. With parts very close to the final geometry (near-net shape), the machining process is drastically reduced as well as the material waste. Allen [10] lists BTF rates ranging from 6 to 20 for manufacturing titanium aeroengine components by its conventional routes and presents a 30% cost reduction after using WAAM, while Barnes et al. [9] reports an industry average BTF of 11 for machined parts and about 21 for titanium forgings; in contrast, using WAAM, the same obtained a BTF of 1.5 and ~48% reduction of total costs. According to Williams et al. [5], for the WAAM process using GMAW, the deposition rates are high enough, which makes it possible to manufacture large-scale parts in reasonable times. With rates ranging from 1 to 4 kg/h for aluminum and steel wires, most parts can be manufactured within one working day. Some parts can even be obtained with higher deposition rates (for example, 10 kg/h), but some geometric and metallurgical characteristics can be compromised.

The effects of sudden thermal cycles on a metal alloy can cause changes in its microstructure, generating structures with different mechanical properties. In a welded region, due to heat, there is a molten region and regions that have undergone solid state transformation, such as a region of grain growth and a region of total and partial grain refinement, called the HAZ. In additive manufacturing, the expected microstructure is similar to that of a multipass joint; the melted zone is once again fused, and, due to the thermal cycles to which the region is again exposed, a new HAZ

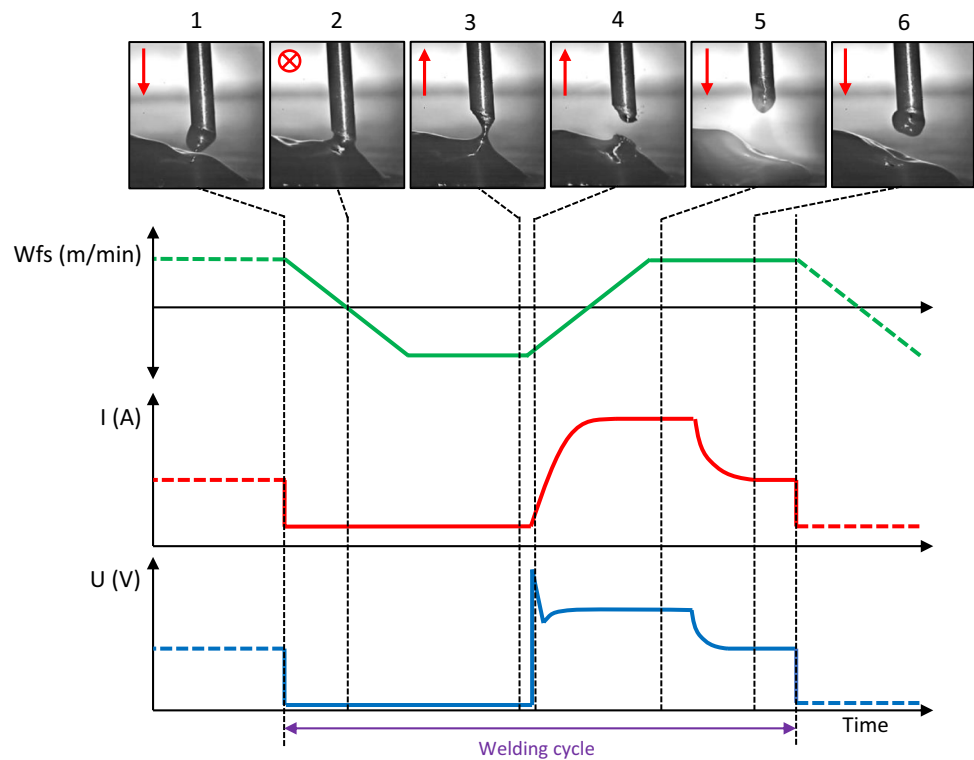
is formed. In the coarse-grain region of the HAZ, due to heating, there is grain refinement and a new CG HAZ near the melt zone. This heterogeneity in the microstructure generates oscillations in the hardness profile of the part, as is described by Ali et al. [4] and Kou's book [11]. These microstructural variations caused by sudden thermal cycles can be critical to the mechanical proprieties and overall part quality, mainly in materials susceptible to fragile phases formation. In this regard, the process planning with regard to energy and thermal cycles is imperative to obtain high process efficacy. Oliveira et al. [12] proposed a unified equation to compute the energy density based on power, travel speed, heat source dimension, hatch distance, deposited layer thickness, and material grain size. Through this and similar methods, it is possible to quantify and cluster the different experimental conditions for a range of applications.

Most arc welding-based AM techniques apply the GMAW process in function of its deposition rates, controllability, and versatility. Within the ample domain of GMAW variants, process versions based on short-circuiting metal transfer and mechanically assisted droplet detachment (reciprocating wire; dynamic feeding (DF)) lead the applicability for AM. In this technology, metal transfer occurs through the action of surface tension force coupled with wire electrode pullback synchronized with the current waveform. The forward and backward movement of the wire at high frequencies (> 25 Hz) is generated by a secondary motor integrated in the welding torch (push-pull system). The wire feeder assembly in synchrony with the current control system provides a GMAW DF process with high controllability of the deposited bead geometry and the energy delivered to the workpiece along with a smoother metal transfer with virtually no spatter and little fume generation. The best-known commercial variant is CMT developed by the company Fronius [13].

The main characteristic is the reversal of the wire direction after the short-circuit event. In addition, the current is kept at a low level during this phase. The combination of low current level and wire pullback during the short-circuit phase is favorable for very smooth metal transfer, reducing spatter and fume generation. In this variant, the current level is kept low during the entire short-circuit phase. Figure 1 schematically shows the basic waveform of the CMT process.

Pickin and Young [13] compared the stability of the conventional GMAW process and CMT in the welding of thin aluminum sheets. This work was expanded by Feng et al. [14], and additional studies were performed by Zhang et al. [15]. The main results of the cited studies showed that the CMT variant can provide reduced heat input and increased controllability over the metal transfer when welding aluminum alloys compared to the conventional GMAW process. In addition to aluminum

Fig. 1 Typical current (I) and voltage (U) waveforms and wire movement of the CMT variant of the GMAW process



alloys, studies highlight the use of CMT in welding of nickel alloys and dissimilar joints. Rozmus-Górnikowska et al. [16] characterized the microstructure of Inconel 625 deposited on steel in the form of a coating using CMT. Dutra et al. [17] compared CMT to other GMAW variants, including pulsed AC GMAW, for Inconel 625 cladding applications, with CMT achieving the lowest dilution levels, ideal for metal coating processes. Benoit et al. [18] characterized the process in the welding of Inconel 718. The weldability of this alloy using the CMT process has also been investigated by Cao et al. [19]. In addition, Shang et al. [20] investigated the microstructure and mechanical properties in the joining of dissimilar aluminum-magnesium joints with the CMT process. Thus, the wide scope and applicability of the CMT version have been demonstrated.

Further CMT versions are available, which combine waveforms and deposition strategies such as DC pulsed and AC pulsed. In this context, one can highlight the CMT Pulse version (CMT+P) that combines the current pulses (pulsed metal transfer) with the short-circuit transfer assisted by the dynamic feeding (CMT). The CMT Advanced combines dynamic feeding (reciprocating wire) with electric current polarity variation and the CMT Pulse Advanced version (CMT+P ADV), which, as the name suggests, combines the two aforementioned versions [21, 22]. Throughout this work, more specific information about the applied CMT and its versions will be presented.

In additive manufacturing, Cong et al. [22] compared the effects of different waveforms of the CMT variant (CMT, CMT Pulse, CMT Advanced, and CMT Pulse Advanced) on the porosity formation characteristic of Al-6.3% Cu alloy in additive manufacturing. The obtained results showed that CMT Pulse Advanced proved to be the most suitable process for depositing aluminum alloy due to its excellent performance in controlling porosity. The key factors that enable the process to control the porosity efficiently are the low heat input, a fine equiaxed grain structure, and effective oxide cleaning of the wire.

Analogously, Derekar et al. [23] analyzed the influence of CMT pulse on porosity formation compared to pulsed GMAW process for wall fabrication via additive manufacturing with the aluminum alloy 5183. On the other hand, Ortega et al. [24] investigated the manipulation of the standard CMT waveform for WAAM using Al5Si aluminum alloy. In the production of multilayer parts using titanium (Ti-6Al-4 V), Almeida and Williams [25] compared the use of the conventional GMAW process and its CMT variant for the deposition of single beads at high deposition rates, envisioning its application for large-scale part construction. Using high-strength and low-alloyed steel in part production, Yildiz et al. [26] proposed a mechanical and metallurgical analysis of single- and multi-bead walls using the ER120S-G steel wire and the CMT variant. Similarly, Posch et al. [27] analyzed the mechanical properties of parts made with a duplex stainless steel alloy from the CMT variant of the GMAW process by comparing to casted parts

Table 1 Increment values used in the experiments

	Conventional	CMT	CMT ADV	CMT Pulse
Increment	1.47 mm	1.37 mm	1.48 mm	1.24 mm

of the same geometry. Analogously, Ali et al. [4] analyzed the influence of welding energy on the resulting mechanical properties and microstructure of a tool steel. The investigations were carried out with the hot working tool steel X37CrMoV 5–1, used in the manufacturing of polymer injection molds, hot extrusion dies, and forging dies.

As seen, arc welding-based additive manufacturing has been consistently targeted in research efforts, and further work is needed for the rising of its understanding. The main objective of this work is to compare the effects of each GMAW CMT variants on thin-wall parts build by WAAM technique. In this regard, based on the electrical signals (voltage and current), thermal (IR filming), geometrical, and metallurgical results, a multiple output analysis was carried out in order to evaluate the potentialities, advantages, and challenges of the CMT, CMT Advanced, and CMT Pulse applied to WAAM of martensitic stainless steel, with the GMAW conventional as comparison reference. In addition, the work seeks a contribution to the clarification of the popularized attribute “cold,” granted to some arc welding processes.

2 Experimental procedure

In the practical experiments, thin walls were built using both the synergic conventional GMAW and CMT variants, i.e., CMT, CMT Advanced, and CMT Pulse. The experimental configuration lies on a complex parameterization range, with regard to the nonconventional, very low wire feed speed of 1.7 m/min. This is the lowest possible value in the CMT configuration for all cases and an extreme low for the GMAW process. In order to perform these experiments, an anthropomorphic 6-axis robot model HP20D from Yaskawa was used to move the CMT Robacta torch, coupled with a Fronius welding power source model CMT Advanced 4000R equipped with the configuration interface model RCU5000i.

The ASTM A36 steel plate 12.7 mm thick, 31.75 mm wide, and approximately 200 mm long was used as the substrate for deposition of the strands. The consumable wire used was AISI 420 wire, i.e., martensitic stainless steel; as shielding gas, an active mixture with 95% Ar, 3% CO₂, and 2% N₂ was used. The parameters set for the purpose of comparing the dynamic behavior between the versions of the CMT process were 1.7 m/min wire speed, 30 cm/min welding speed, 12 l/min shielding gas flow, and 15 mm of CTWD.

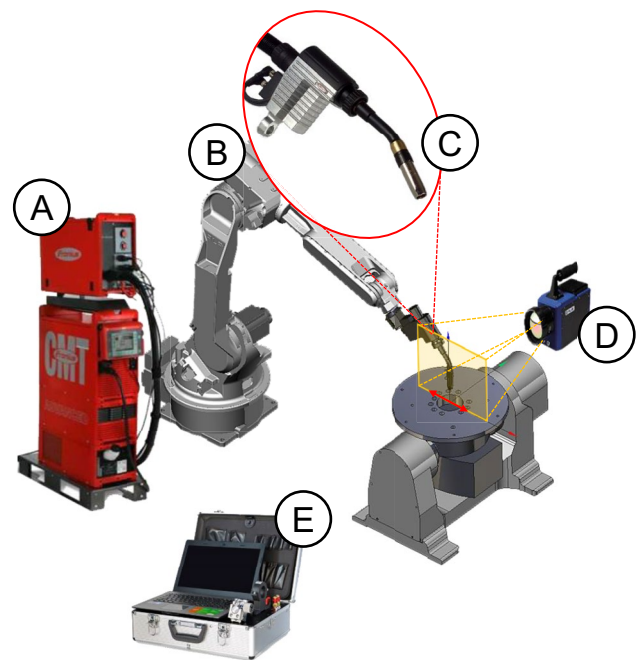
Thirty-five layers were deposited over a length of 150 mm, with the increment between layers equal to the height of the first bead, in order to maintain the same distance between the nozzle and the workpiece. Table 1 shows the increment values used.

**Fig. 2** Schematic representation of the torch path

A bidirectional continuous path was used to build the walls, i.e., with inversion in the welding direction. Figure 2 schematically illustrates the path followed by the welding torch.

The electrical signals (arc voltage and welding current) and wire speed acquisition were executed with a portable acquisition system dedicated to welding, the IMC SAP V4 with an acquisition frequency of 5 kHz. Thermographic filming was performed using a FLIR SC7000 camera with an acquisition rate of 10 Hz. Figure 3 schematically illustrates the arrangement of the equipment and the thermal camera with detail to the region of interest, positioned perpendicularly 1 m away from it.

The temperature measurement was performed in two places. In the first point, the maximum temperature at the center of the deposited layer was observed; when the welding torch reaches the edge of the wall, this method was used on all layers. The second was at a point fixed in the center of the side face of the base plate, and maximum temperature at

**Fig. 3** Schematic representation of the experimental base, where A, power source Fronius CMT Advanced 4000R; B, anthropomorphic robot Motoman HP20D; C, Welding torch Robacta Fronius; D, thermographic camera FLIR SC7000; E, data acquisition IMC SAP V4

the substrate was observed over the time. Figure 4 schematically illustrates the method adopted for the measurement.

Metallographic analysis was carried out by cutting the samples in the central region, extracting a 15 mm sample, as shown in Fig. 5. Then, sanding was performed in the following order: 80, 120, 320, 400, 600, and 1200 sandpaper granulometries and polishing with 1- μm alumina. The etching was performed with marble reagent (4 g $\text{CuSO}_4 + 20 \text{ ml HCl} + 20 \text{ ml H}_2\text{O}$); the etching time was 5 s. An Olympus BX60 trinocular optical microscope at $200\times$ resolution was used to check the microstructure of the samples.

Microhardness measurement was conducted along the central region of the wall, following the line demarcated in Fig. 6, using 0.2 kgf pre-load, an indentation time of 10 s as suggested by ASTM E92 [28] and an increment of 0.5 mm, starting at 1 mm from the baseline P_0 (point of greatest penetration). The aim of this test was to verify the effect of the deposition thermal cycles in the hardness along the sample vertical axis, since the wall was built without stop time. In addition, a comparison between the CMT variants was realized evaluating the waveform effect on the hardness.

3 Results and discussion

Each CMT variant of the GMAW process has distinct characteristics that confer a unique dynamic behavior to the molten pool. In CMT, there is electromechanical control of the metal transfer, i.e., both the control of the electric current and the wire feed dynamic. During the short circuit, the wire speed becomes negative, i.e., the pullback of the electrode wire occurs to assist the droplet detachment by surface tension while in low welding current values. This dynamic avoids arc reopening at high welding current, preventing power peaks, which tend to generate spatter and instabilities in the process [21]. In addition, this strategy promises a reduced heat input compared to the conventional GMAW process [13–15].

In the wall construction, for the conventional GMAW process, an average welding current of 81 A was obtained,

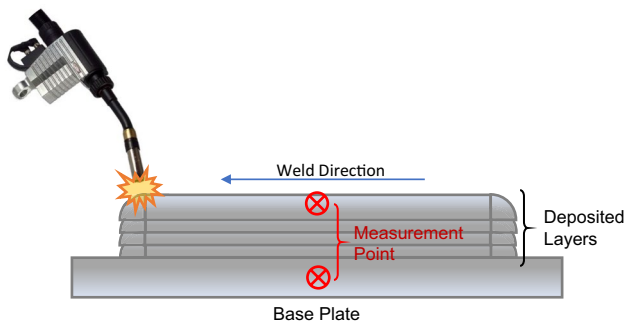


Fig. 4 Schematic representation of the temperature measurement

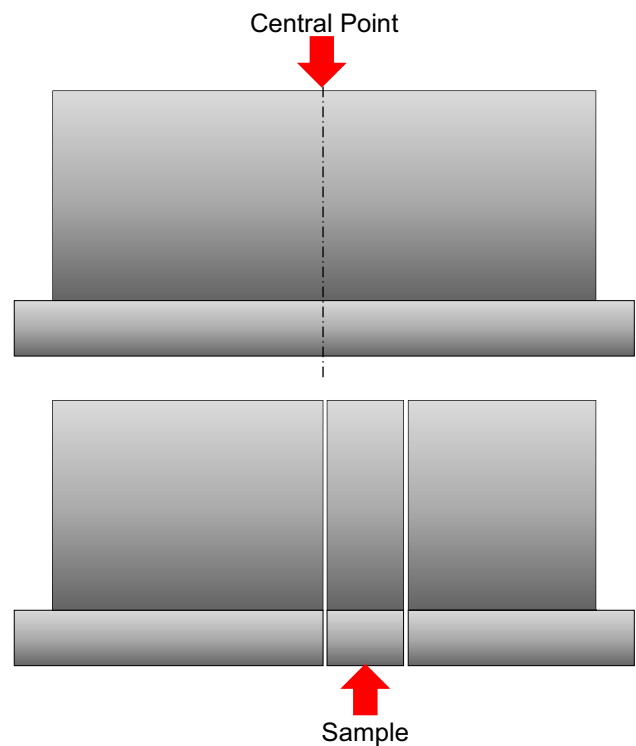


Fig. 5 Schematic representation of sample cut in wall center point

while for the CMT variant, a value of 66 A was verified, about 12% lower. Figure 7 illustrates the oscillogram of the arc voltage and welding current behaviors, with detail to the steps of the process where the detachment of droplets occurs and the consequent reopening of the electric arc.

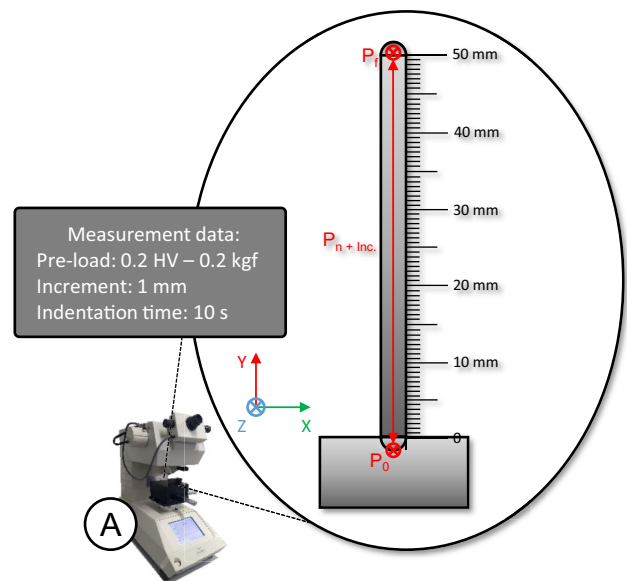


Fig. 6 Schematic representation of Vickers hardness measurement and the main test data. A HMV SHIMADZU micro hardness tester

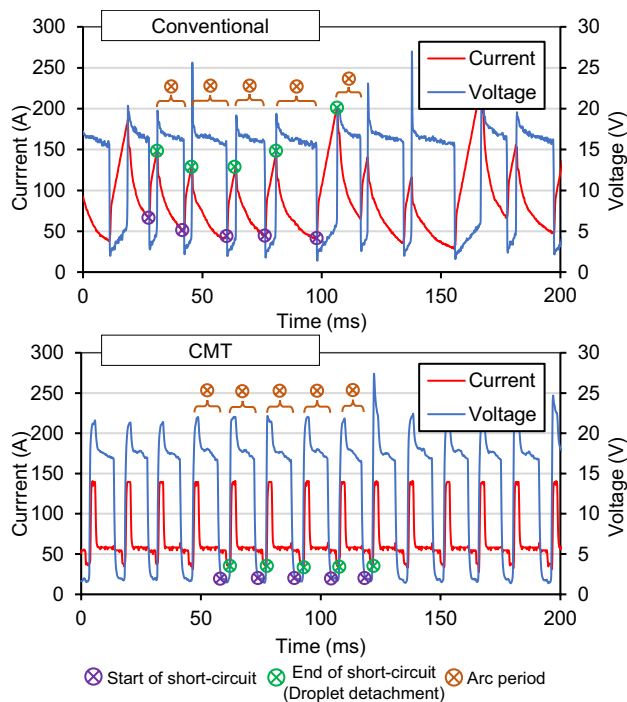


Fig. 7 Oscillogram of the welding current and arc voltage behavior of the GMAW conventional process and CMT variant

The CMT version, even with a lower average current value compared to the conventional one, does not present a significant difference in power value, with only 10 W of variation, with 985 W for the conventional and 995 W for the CMT. This effect is due to the detachment frequency, which is higher for CMT. However, the instantaneous power at the time of arc reopening is 75% lower for the CMT process, precisely because of the combination of wire movement and current modulation control, as can be seen in the power oscillogram in Fig. 8.

However, based on this test, it can be stated that electro-mechanical control of the metal transfer results in increased process stability and reduced current peaks during arc reopening with significantly reduced spatter production. This result reinforces what some researches have been showing, where in some cases, the CMT version does not present lower heat input in relation to the conventional GMAW process, and its thermal efficiency is equivalent in relation to the same [4, 22, 23, 29].

Another CMT version evaluated in this work was the CMT Pulse. The typical CMT Pulse waveform is depicted in Fig. 8, which presents the voltage and current oscillograms obtained from the experiments in the scope of this paper. This current waveform presents a combination of two metal transfer modes, namely, short-circuiting metal transfer (supported by dynamic feeding) and pulsed metal transfer (with droplet detachment during the base current). All phases of the CMT Pulse waveform have been flagged with markers in Fig. 9.

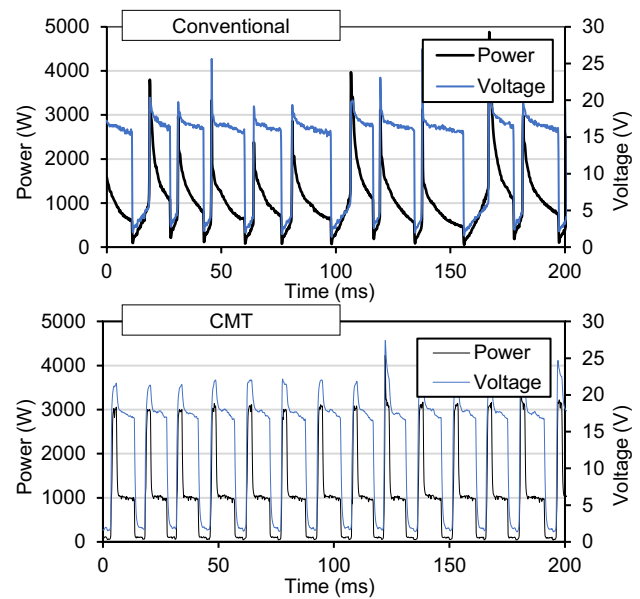


Fig. 8 Power and arc voltage oscillograms of the conventional GMAW and CMT processes

It is possible to verify a pronounced power value during the current pulse, about 65% higher than the current pulse in the CMT during arc period, totally predictive since the metal transfer mode is different. Nevertheless, the overall power value measured was 1160 W, about 15% higher than CMT and conventional. Figure 10 shows the power oscillogram of this process.

The last CMT version evaluated has been the CMT Advanced. The typical current waveform is showed in Fig. 11 which contains the arc voltage and welding current oscillograms. In this version, variable polarity is used. The current waveform can be divided into two parts, positive and negative phase. For both phases, the metal transfer occurs through short circuit with pullback wire movement

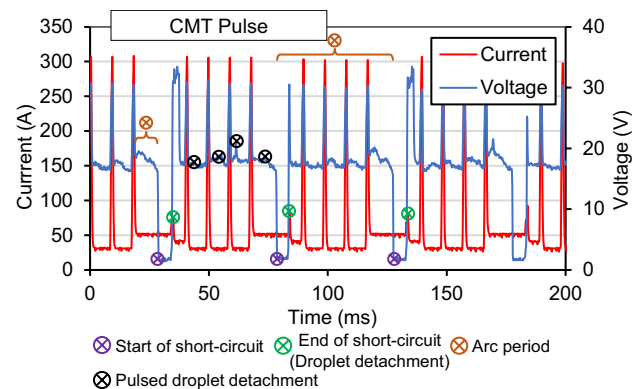


Fig. 9 Welding current and arc voltage oscillograms of the CMT Pulse variant

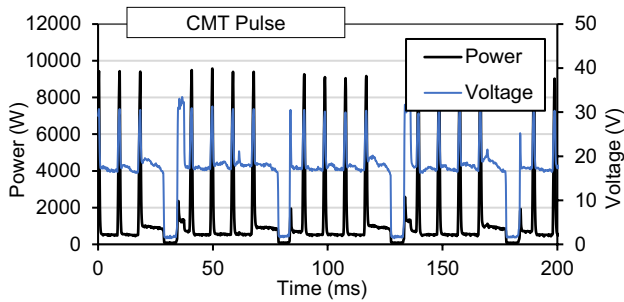


Fig. 10 Power and arc voltage oscillograms of the CMT Pulse variant

or dynamic feeding. However, in the negative phase, a lower current intensity than in the positive phase is used. This fact occurs since in the negative current (wire electrode negative), the melting rate is higher compared to the positive phase. In summary, using negative current requires less current than positive current to melt the same amount of material and, consequently, a low power results.

In relation to the other GMAW variants already mentioned, the CMT Advanced presented the lowest power, about 866 W. This value was calculated using the absolute welding current and voltage values in order to be compared with others. This power reduction is due to the polarity inversion for a certain period combined with the electrode pullback generated by the DF (dynamic feeding) technique, which substantially reduces the reopening with highest welding current. The effect obtained with negative polarity ends up increasing the wire melt rate, since this polarity concentrates most of the heat at the electrode. This increase in the melting rate is reflected by lesser power required to melt the filler material, when maintaining the same wire feed speed. These claims can be verified in the welding current-arc voltage oscillograms (Fig. 10) or the power graph shown in Fig. 12.

After measuring the average power levels, it is possible to order which variants tend to impose more heat on the part,

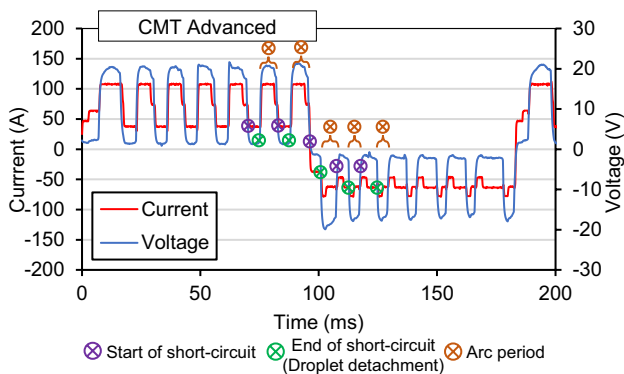


Fig. 11 Welding current and arc voltage oscillograms of the CMT Advanced variant

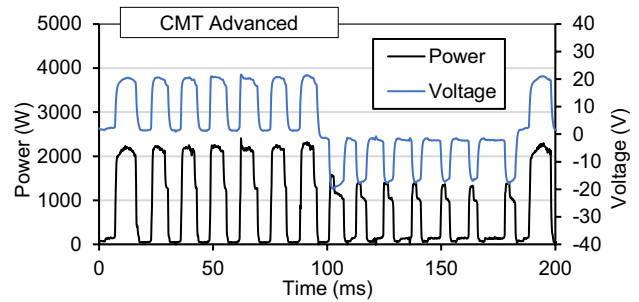


Fig. 12 Power and arc voltage oscillograms of the CMT Advanced variant

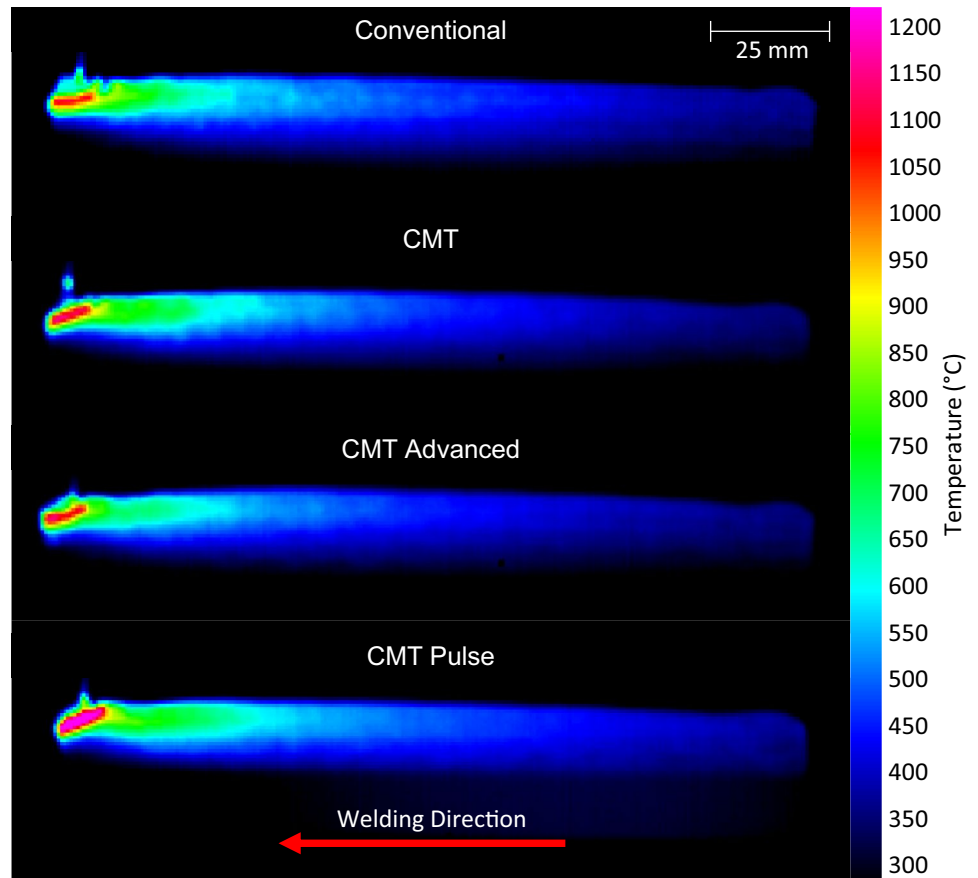
enriching the subsequent temperature analysis. In order to obtain parts using the WAAM technique is necessary to align the virtual increment with the true increment of the layers, in other words, adjusting the height of the layer based on the part already built. This adjustment is greatly influenced by heat buildup, which in turn changes geometric characteristics of the weld bead throughout the fabrication of the part, as was observed in the works of Ali et al. [4], Derekar et al. [23], Venturini et al. [2], and Posch et al. [27].

For each feed rate, there is a minimum amount of energy required to melt, deposit, and maintain the heated region; the surplus is dissipated to the environment as a function of process efficiency [29]. In the case of the GMAW process and the CMT versions, according to Arevalo and Vilarinho [30], the thermal efficiency for these processes is about 76%. In this sense, the higher the welding energy for the same feed rate, the greater the excess energy dissipated. This excess heat, in turn, tends to generate distortions and undesired conditions in the microstructure [31].

In order to evaluate the influence of heat input in additive manufacturing with the different CMT versions, infrared filming of the wall construction was performed. Figure 13 illustrates the thermal profile obtained with the filming, where a more significant difference can be seen only for the CMT Pulse version.

Based on the data from the infrared filming, the graph in Fig. 14 was constructed. It was found that all versions reached a temperature quasi steady state around 400 s of operation, sufficient time for the construction of 14 layers. From this point on, the test pieces presented low temperature variation, indicating balanced energy throughput, with energy lost from convection to the environment and conduction to the workpiece. In this transient state, it is noticeable that the conventional process heats up at a relatively higher rate than the others; however, it is considered that the difference is not significant. In the quasi steady state, the CMT Pulse version reaches a higher value than the others, around 780 °C, while for the conventional process, the average was 732 °C, for the pure CMT 735 °C, and for the CMT Advanced, the average was 702 °C.

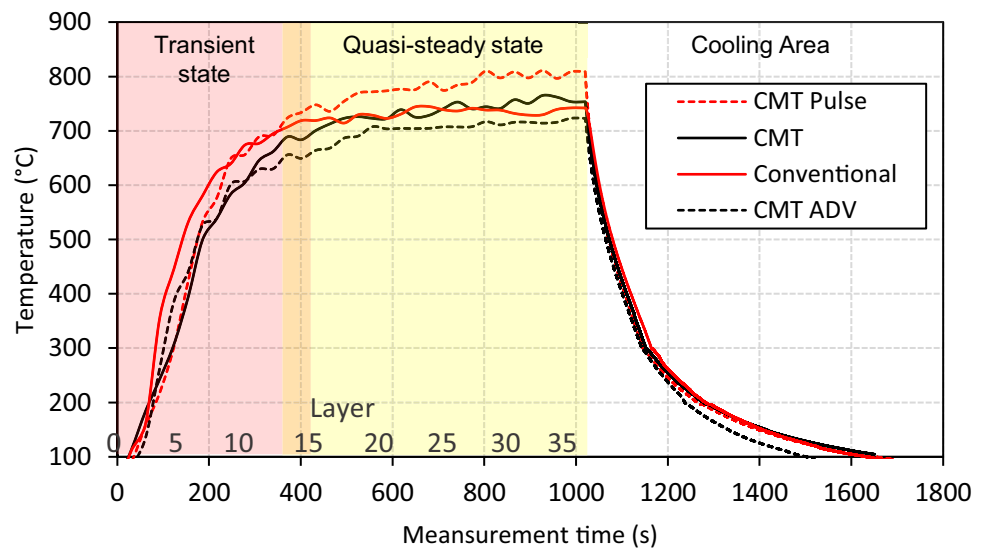
Fig. 13 Thermal profiles obtained with thermal imaging (layer 20)



According to the temperature information obtained, it is possible to verify that the biggest difference is between the CMT Pulse and Advanced versions, representing a variation of about 80 °C. For the conventional and CMT versions, the difference is not considered significant, which, in a way, contradicts the statement puts forward by some authors that

CMT is “cold.” What can indeed be stated is that the CMT could be considered the version with greater stability in metal transfer. This fact can be qualitatively observed in the voltage x current (cyclogram) shown in Fig. 15. The cyclogram is primarily a qualitative method to evaluate overall stability of arc welding processes (quantitative analyses are

Fig. 14 Time–temperature wall build-up behavior



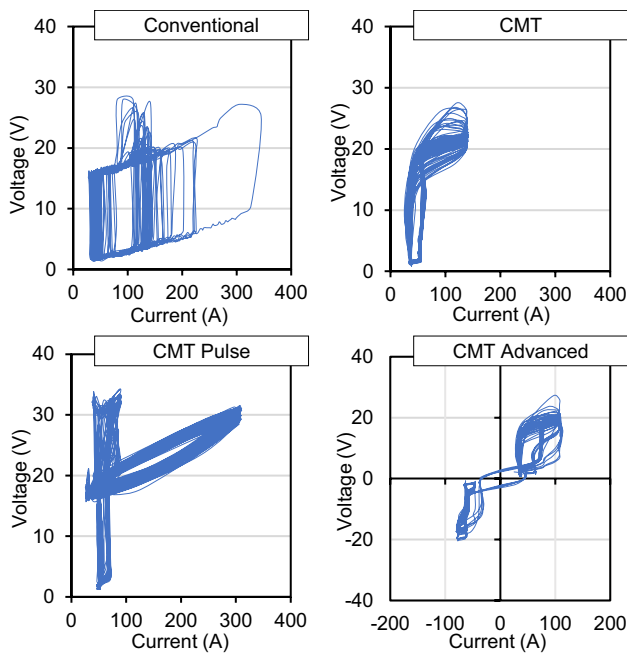


Fig. 15 Cyclograms of the tested GMAW variants

also possible through proper data treatment). The method consists of the analysis of voltage and welding current signals over time. The welding current is plotted cyclically, for all metal transfer/droplet detachment event as a function of the voltage, thus representing a static arc characteristic. The concentrated superimposition of measured current \times voltage signals indicates greater similarity/regularity of the detachment cycles, thus translating greater process stability. The conventional process has a lower stability due the lack of coincidence and regularity in its cyclogram. The

CMT and its variants, on other hand, present high stability since the cyclogram exhibits higher regularity. This is mainly due to the highly controllable electromechanical transfer mode.

Another parameter observed was the temperature of the substrate along the wall construction. After 250 s of the beginning of the process, there was a loss of influence of the base material on the heat exchange of the outer layers, basically from the tenth layer on. The other singular observation was the difference in maximum base temperature obtained when welding with the CMT compared to the conventional one, about 50 °C, while the temperature of the CMT Advanced and conventional CMT showed no significant difference. In addition, the CMT Pulse temperature continued to show higher values than the others, as illustrated in Fig. 16. Each ripple present in the graph represents the arrangement of a new layer.

The hypothesis for the higher temperature of the base plate presented in the CMT in relation to the conventional is that the cycloramas dynamic feeding promoted by the CMT fosters the convective effect on the weld pool due to its enhanced oscillation. This increases the thermal exchange of the weld pool with the rest of the part, reflecting in the higher temperature in the base plate, even though the CMT presents less power than the conventional [11, 21].

The morphology of each constructed wall was influenced by the different bead geometries that each process produced. Figure 17 shows the morphology obtained in the walls.

The graphs in Fig. 18 illustrate the difference between wall-height measurements. The conventional and CMT Advanced versions showed no significant difference in wall height between each other, since they present 50.07 mm and 50.22 mm average height, respectively. However, it can be

Fig. 16 Temperature behavior of the base plate

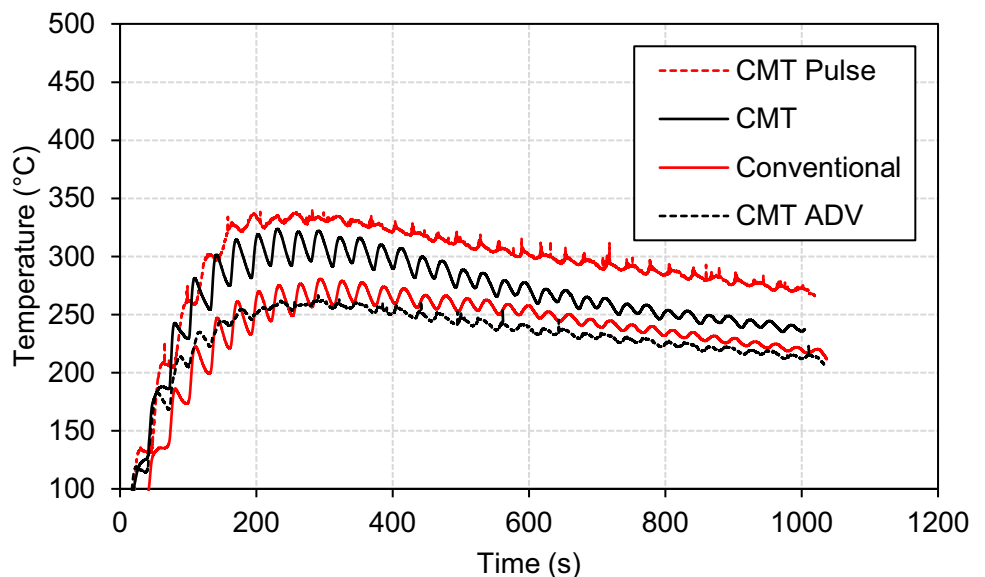
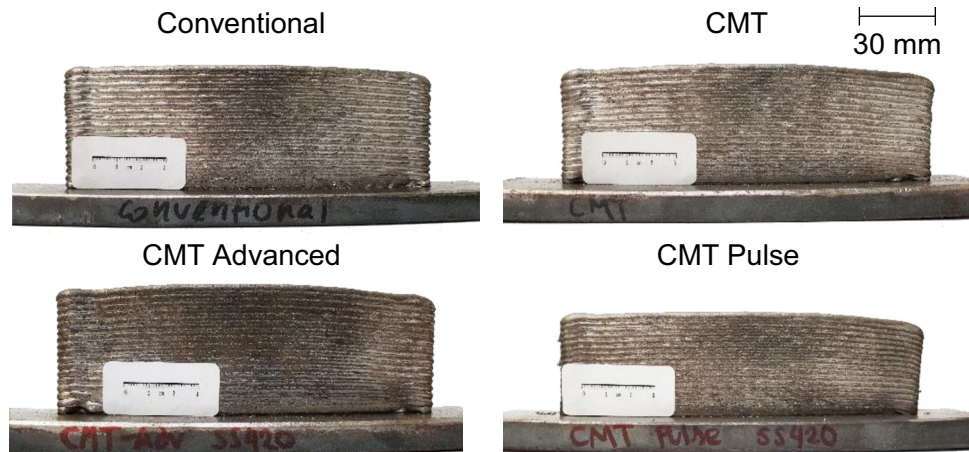


Fig. 17 Morphology obtained on the walls



seen that the CMT and CMT Pulse versions, due to the bead geometry, showed lower wall average height after 35 layers, about 46.43 mm for CMT and 42.28 for CMT Pulse.

These differences corroborate with the temperature results (Figs. 13, 14, and 16), where the described effect resulted in significant modification of the part geometry. One possible explanation to these results concerns the greater welding pool agitation promoted by CMT versions when compared to the conventional process, forcing not only higher heat transfer to the test piece (Fig. 13) but also greater welding bead width or wall thickness, thus lowering the wall height (Fig. 18).

The CMT Advanced presented results indicate the opposite behavior, mainly because this process uses alternated welding current. The variable polarity current promotes decreasing the amount of heat input to the test piece while increasing the wire feed speed in order to maintain the same arc length for the same average welding current as seen observed in the Figs. 13, 14, and 16.

For a better visualization of the height variation of the walls, a cross section of the central region of the wall was used; see Fig. 19, where the height variation is clear.

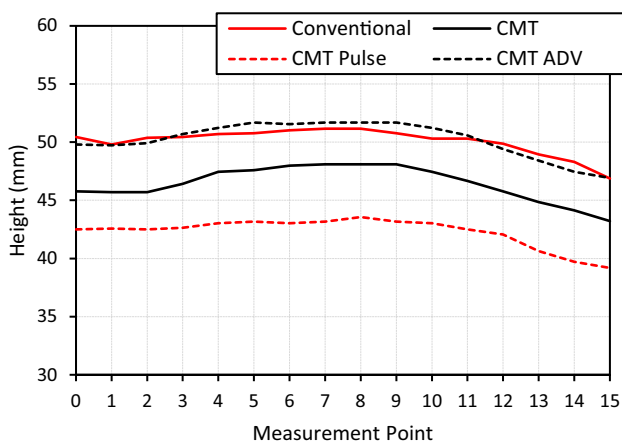


Fig. 18 Variation of wall height as a function of welding processes

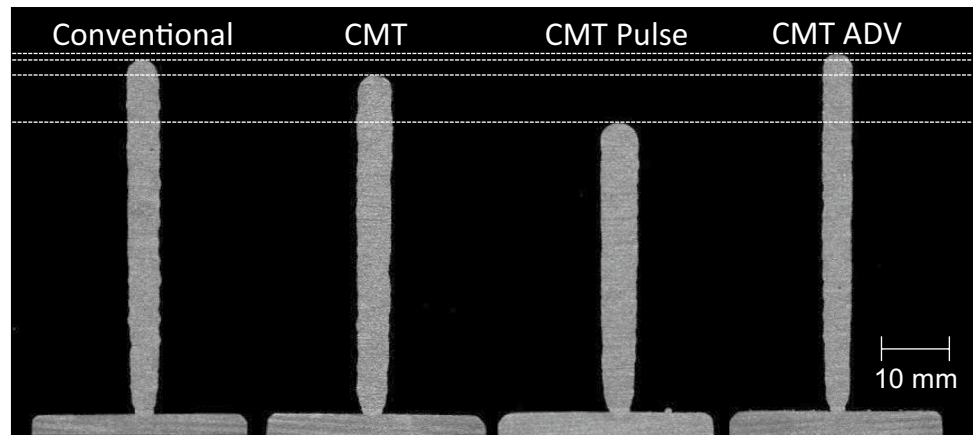
The graphic in Fig. 20 was constructed with basis on the analysis of the variation of the wall height through the error relative to the mean value, where it is possible to observe the surface undulation of the walls, as well as its variation relative to the mean value. The largest wall-height error observed is at the end of the weld bead (layer), and this occurs due to the increase in heat input throughout the deposition. This increasing heat modifies the bead geometry slightly by decreasing its height and increasing its thickness at the end of the wall (higher overall temperature leads to higher molten metal fluidity and lower surface tension). This effect is enhanced by the torch idle time at the end of the wall during the movement reversal. This error tends to be cumulative and irreversible along the wall height, since the variation of the bead height can indirectly influence arc length, thus increasing the power and with it the heat involved in the process at that instant. This hypothesis can be validated by observing the wall height at each layer's beginning and ending, along with the arc power behavior.

This effect generates a flattening of the bead ending region (negative error). Along with this, in the central region, due to the bending of the base plate by the heat input, there is a contraction of the weld bead, which ends up being distorted and generating a greater positive error in the center.

Based on these findings, it is possible to verify the need for over-material, in order to better meet the previously specified dimensions, placing the part in a near-net-shape position, just as Ali et al. [4] consider in their work. In this sense, in a process, planning a usable zone should be defined for the workpiece, where the exceeding part will be removed in post-processing machining. Another alternative is to create techniques to compensate for distortions online by changing the deposition rate or welding speed.

The wall thickness was also analyzed. Each process variant has presented single beads with different geometries for the same wire feed speed, both in height and width. These single bead characteristics influence the appearance of the wall as they are overlaid on top of each other, in particular

Fig. 19 Cross section of the central region of the walls



the resulting thickness of the wall. A priori, it can be noted that the increase in power significantly influences the single beads height and width, in consequence the wall thickness. From the methodology presented, cross-section measurements showed significant variation in the average thickness along the cross sections, where the CMT Advanced showed lowest thickness, about 4 mm. For the weld bead deposited by the CMT Pulse, a thickness of 5 mm was obtained, while the CMT variant resulted in a value of 4.5 mm and for the conventional a value of 4.3 mm, as can be seen in Fig. 21.

All processes presented low relative standard deviation, where only CMT Pulse presented 3% more than the others, as can be seen in the graph of Fig. 22.

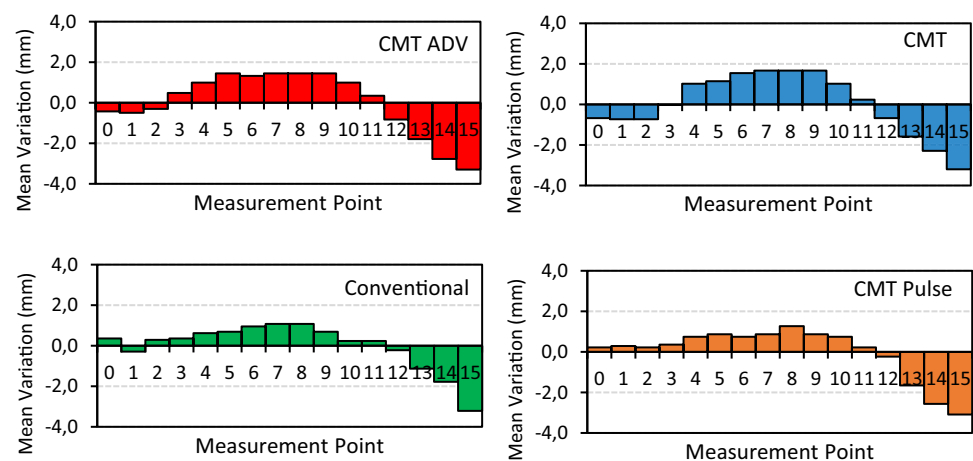
Therefore, relating the geometric characteristics observed on the wall to the power, it can be seen that the power has a significant influence on the thickness, since increasing the power increases the energy involved in the process which, at the same deposition rates, causes greater wetting and bead width and lower bead height.

In addition, it was evaluating the effective area using the sample from the central wall region. It can be noted the CMT Advanced presented the lower effective thickness, around 3.9 mm; for CMT and conventional, the values measured

were 4.5 mm and 4.3 mm, respectively. The CMT pulse presented an effective thickness of 4.9 mm. However, aiming a greater evaluation of the effective thickness, the effective area was calculated, the measurement considered the highest effective thickness without exceeding wall edges, but for fitting, the greater effective thickness was necessary to ignore the first 3 mm of the wall, where the thickness is extremely thinner than the rest of the wall. Therefore, for Conventional, CMT, and CMT pulse, the effective area was 84% of the wall total area; on other hand, in the CMT Advanced, the effective area was 86% of the wall total area. Figure 23 shows the effective area measured in contrast to the wall total area. Results show that the CMT Advanced has a greater geometrical constancy throughout time, i.e., a lower wall thickness variation.

In the samples built by additive manufacturing, a macrostructure similar to multipass welding was obtained, but with a single column, as shown in Fig. 24. In these macrographs, it is possible to observe the region where the remelting of the layer occurred by means of the light-colored transversal line, which represents the interface between the HAZ and the remelted zone. For the Conventional, CMT and CMT Advanced are clear the layer

Fig. 20 Relative error of the height of the walls as a function of the reference



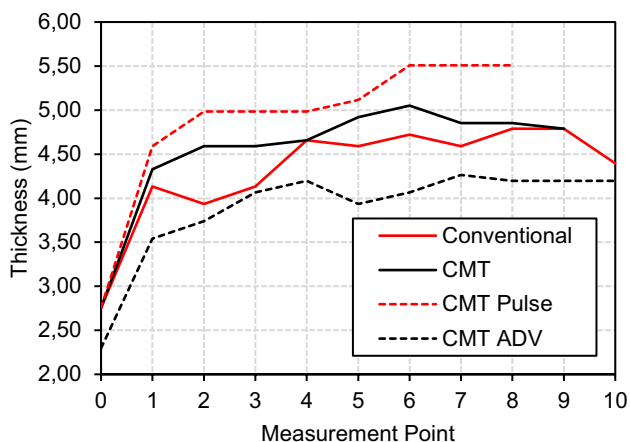


Fig. 21 Thickness variation along the wall cross section

interface while for the CMT pulse the remelting is intense enough to hide the layer interface showing only a slight HAZ.

The microstructure observation evidenced the prominence formation of columnar dendritic grain. Their morphology was quite homogeneous for each variant. The microstructure comparison between the samples, as shown in Fig. 25, exhibits for the CMT Advanced a refined structure while for the CMT Pulse variant a slightly coarser morphology. The other two variants, CMT and Conventional, presented a morphology slightly refined, without significant difference with each other.

According to Kou [11], with increasing cooling speed, there is an increase in the magnitude of thermal subcooling that can be achieved. With this, the nucleation rate of the solid is increased and, as a result, grain refinement. This is verified for the CMT Advanced process, which presented

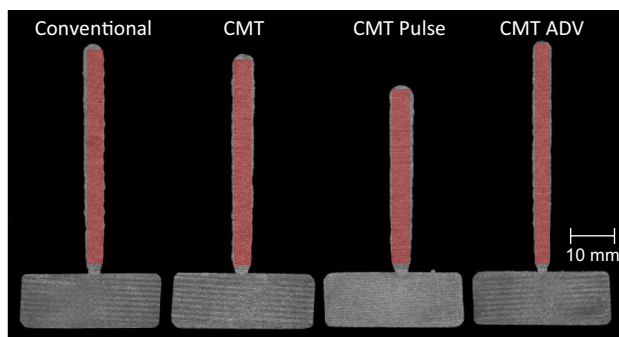


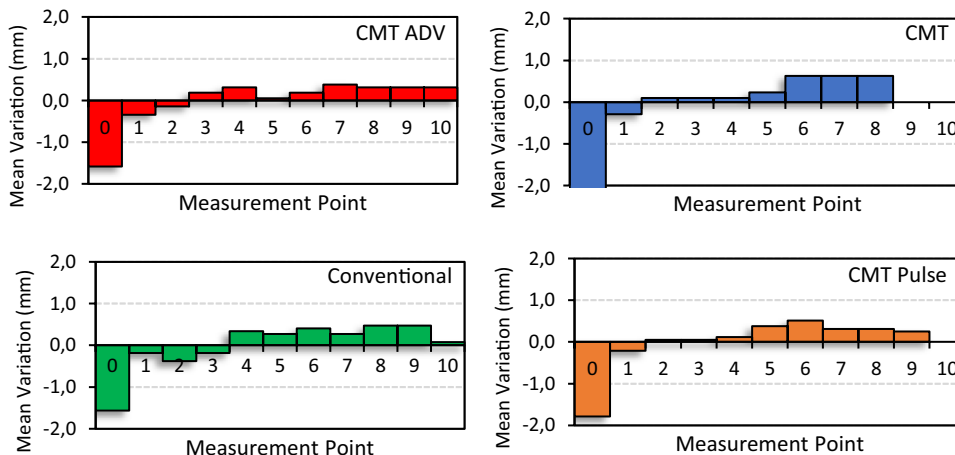
Fig. 23 The effective area measured in contrast to the wall total area

smaller grains in relation to the others. Conversely, the CMT Pulse showed larger grains. This statement corroborates the results found regarding the temperatures and average power of the processes. This was also verified from the heat input calculation, taking into account what was suggested by Averaldo and Vilarinho [30], where the suggested efficiency for the conventional process was 70%, while 76% for the CMT variants was used, as shown in Table 2.

Another factor that may be influential on these results is the tempering or reheating of these dendritic grains due to multipass welding. Due to the temperature reached above A1, microstructural modifications were possible, i.e., grain growth, seen in the CMT Pulse process.

Among the processes, the CMT Pulse presented higher values of hardness, with an average of 506 HV; this result was expected, since its cooling rate was higher, as well as its thermal contribution. In the wall built from the CMT process, the average was 420 HV, for conventional 428 HV and for CMT Advanced 438 HV, as shown in the graph of Fig. 26. Based on these results, it is possible to see a tenuous relationship of the average hardness with the heat input. These results corroborate with Ali et al. [4] and Posch et al. [27].

Fig. 22 Relative error of wall thickness as a function of the average thickness



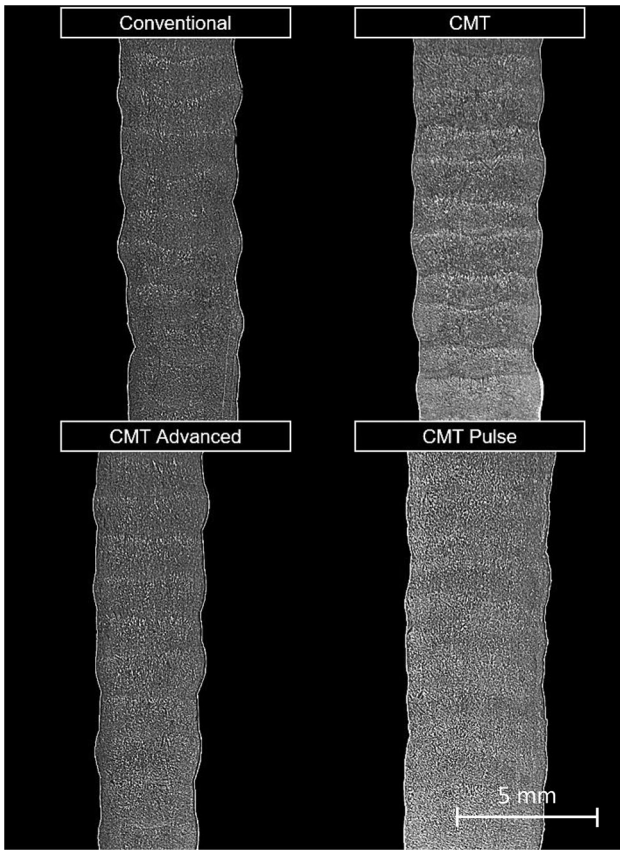


Fig. 24 Macrograph of the central region of the cross section of the walls built by WAAM

Table 2 Heat input

Process	Power (W)	Weld speed (cm/min)	Heat input (kJ/cm)
Conventional	985	30	20.68
CMT	995	30	22.68
CMT ADV	866	30	19.74
CMT Pulse	1160	30	26.45

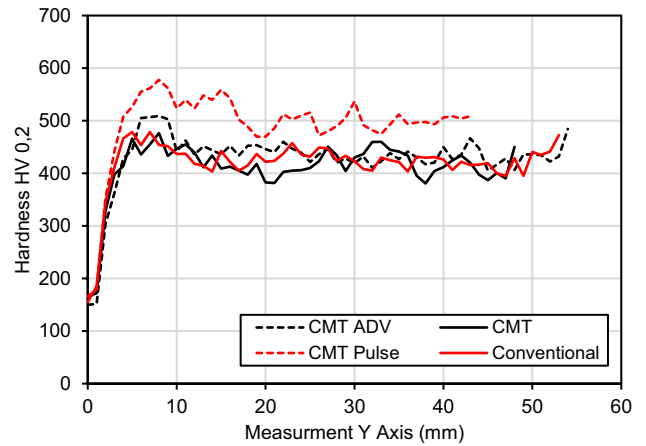
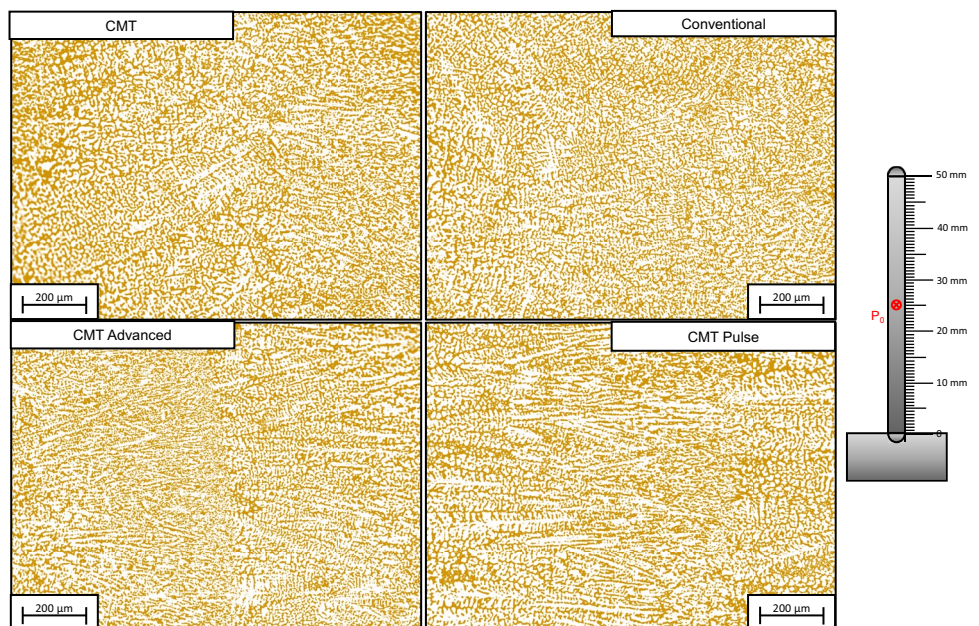


Fig. 26 Hardness along the cross section

Fig. 25 Microstructure recorded in the central region of the samples' cross section



4 Conclusion

In this study, a comparison was made between variants of the GMAW process in the manufacturing of thin walls with single-pass layers, using the WAAM technique with martensitic stainless steel wire (AISI 420). These versions of the GMAW process have electronic control of the current and dynamic wire feeding. From practical tests, analysis of the electrical variables, thermal behaviors, and the morphology of the walls built, the following can be concluded:

- All assessed GMAW technologies (conventional GMAW, CMT, CMT Advanced, and CMT pulse), for the conditions of the present work, showed applicability for additive manufacturing operations, based on good wall geometric characteristics.
- The conventional GMAW process, in relation to the others, did not present significant difference in morphology, as could preliminary be anticipated. Notwithstanding, it was possible to notice a lower arc stability in comparison with the CMT versions, which lead to a greater control of the finished dimensions and metal transfer and, hence, to material and process efficiency and productivity for the latter.
- The CMT Pulse process, due to the amount of energy imposed to the part, generated the highest values of temperature and, consequently, highest cooling rate, which reflected on the average hardness of the wall material. Another consequence of the higher energy was the lower weld bead height compared to the other processes. This caused the walls to have the lowest overall height, for the same number of weld beads deposited as the other processes.
- The CMT Advanced presented the lowest heat input due to the variable polarity (AC) waveform. The AC improves the wire-melting rate as the negative current has a higher wire-melting capability than the positive phase. Therefore, regarding WAAM applications, CMT Advanced tends to be more efficient than the other evaluated GMAW versions, since it uses less energy and lower average welding current to obtain the same average wire-melting rate while still obtaining the same average wall hardness.

Acknowledgements The research proposed in this paper was supported by LABSOLDA — Welding and Mechatronics Institute and Federal University of Santa Catarina.

Author contribution DG conducted the experimental procedures and was responsible for writing the paper; RHGeS contributed to the paper structure, methodology, and did the final proofreading and writing refinement; PCJR assisted the experimental procedures and proofreading; MBS provided literature and was co-responsible for writing the paper; and ABV provided literature, methods, and experimental support.

Availability of data and material The raw and processed data required to reproduce these findings cannot be shared at this time as the data also forms part of an ongoing study.

Declarations

Ethics approval Not applicable.

Consent to participate All authors have approved to participate.

Consent for publication The manuscript was approved by all authors for publication.

Conflict of interest The authors declare no competing interests.

References

1. Hoefler K, Haelsig A, Mayr P (2018) Arc-based additive manufacturing of steel components comparison of wire and powder based variants. *Welding World – Int J Mater Join* 2(62):243–247. <https://doi.org/10.1007/s40194-017-0527-9>
2. Venturini G, Montevocchi F, Bandini F, Scippa A, Campatelli G (2018) Feature based three axes computer aided manufacturing software for wire arc additive manufacturing dedicated to thin walled components. *Addit Manuf* 22:643–657. <https://doi.org/10.1016/j.addma.2018.06.013>
3. Wu B, Ding D, Zengxi P, Cuiuri D, Li H, Han J, Fei Z (2017) Effects of heat accumulation on the arc characteristics and metal transfer behavior in wire arc additive manufacturing of Ti6Al4V. *J Mater Process Technol* 250:304–312. <https://doi.org/10.1016/j.jmatprotec.2017.07.037>
4. Ali Y, Henckell P, Hildebrand J, Reimann J, Bergamann J, Barnikol-Oettler S (2019) Wire arc additive manufacturing of hot work tool steel with CMT process. *J Mater Process Tech* 269:109–116. <https://doi.org/10.1016/j.jmatprotec.2019.01.034>
5. Williams S, Martina F, Addison A, Ding J, Pardal G, Colegrove P (2016) Wire + arc additive manufacturing. *Mater Sci Technol* 7(32):641–647. <https://doi.org/10.1179/1743284715Y.0000000073>
6. Ding D, Pan Z, Cuiuri D, Li H (2015) Wire-feed additive manufacturing of metal components: Technologies, developments and future interests. *Int J Adv Technol* 81:465–481. <https://doi.org/10.1007/s00170-015-7077-3>
7. Cunningham C, Flynn J, Shokrani A, Dhokia V, Newman S (2018) Invited review article: Strategies and processes for high quality wire arc additive manufacturing. *Additive Manuf* 22:672–686. <https://doi.org/10.1016/j.addma.2018.06.020>
8. Horgar A, Fostervoll H, Nyhus B, Ren X, Eriksson M, Akselsen O (2018) Additive manufacturing using WAAM with AA5183 wire. *J Mater Process Technol* 259:68–74. <https://doi.org/10.1016/j.jmatprotec.2018.04.014>
9. Barnes J, Kingsbury A, Bono E (2016) Does low cost titanium powder yield low cost titanium parts? *PowderMet 2016 International Conference on Powder Metallurgy*. Boston, MA: [s.n.]
10. Allen J (2006) An investigation into the comparative costs of additive manufacture vs. machine from solid for aero engine parts. RTO-MP-AVT-139
11. Kou S (2002) *Welding Metallurgy*. 2nd. ed. [S.l.]: Wiley-Interscience
12. Oliveira JP, Santos TG, Miranda RM (2020) Revisiting fundamental welding concepts to improve additive manufacturing: from theory to practice. *Prog Mater Sci* 107(07). <https://doi.org/10.1016/j.pmatsci.2019.100590>

13. Pickin C, Young K (2006) Evaluation of cold metal transfer (CMT) process for welding aluminium alloy. *Sci Technol Weld Join* 11(5):583–585. <https://doi.org/10.1179/174329306X120886>
14. Feng J, Zhang H, He P (2009) The CMT short-circuiting metal transfer process and its use in thin aluminium sheets welding. *Mater Des* 5(30):1850–1852. <https://doi.org/10.1016/j.matdes.2008.07.015>
15. Zhang H, Feng J, Zhang B, Chen J, Wang L (2009) The arc characteristics and metal transfer behaviour of cold metal transfer and its use in joining aluminium to zinc-coated steel. *Mater Sci Eng A Struct* 499(1):111–113. <https://doi.org/10.1016/j.msea.2007.11.124>
16. Rozmus-Górnikowska M, Cieniek L, Blicharski M, Kusinski J (2014) Microstructure and microsegregation of an Inconel 625 weld overlay produced on steel pipes by the cold metal transfer technique. *Arch Metall Mater* 59(3):1081–1084. <https://doi.org/10.2478/amm-2014-0185>
17. Dutra J, Silva R, Marques C, Viviani A (2016). A new approach for MIG/MAG cladding with Inconel 625. *Welding World* 60(6). <https://doi.org/10.1007/s40194-016-0371-3>
18. Benoit A, Jobez S, Paillard P, Klošek V, Baudin T (2011) Study of Inconel 718 weldability using MIG CMT process. *Sci Technol Weld Join* 16(6):477–482. <https://doi.org/10.1179/1362171811Y.0000000031>
19. Cao R, Sun J, Chen J, Wang P (2014) Weldability of CMT joining of AA6061-T6 to boron steels with various coatings. *Weld J* 93(6):193S–204S
20. Shang J, Wang K, Zhou Q, Zhang D, Huang J, Li G (2012) Microstructure characteristics and mechanical properties of cold metal transfer welding Mg/Al dissimilar metals. *Mater Des* 34:559–565. <https://doi.org/10.1016/j.matdes.2011.05.008>
21. Kah P, Suoranta R, Martikainen J (2013) Advanced gas metal arc welding processes. *Int J Adv Manuf Process* 67(1–4):655–674. <https://doi.org/10.1007/s00170-012-4513-5>
22. Cong B, Ding J, Williams S (2015) Effect of arc mode in cold metal transfer process on porosity of additively manufactured Al-6.3% Cu alloy. *Int J Adv Manuf Technol* 76(9–12):1593–1606. <https://doi.org/10.1007/s00170-014-6346-x>
23. Derekar K, Addison A, Joshi S, Zhang X, Lawrence J, Xu L, Melton G, Griffiths D (2020) Effect of pulsed metal inert gas (pulsed-MIG) and cold metal transfer (CMT) techniques on hydrogen dissolution in wire arc additive manufacturing (WAAM) of aluminium. *Int J Adv Manuf Technol* 107:311–331. <https://doi.org/10.1007/s00170-020-04946-2>
24. Ortega A, Galvan L, Deschaux-Beaume F, Mezrag B, Rouquette S (2018) Effect of process parameters on the quality of aluminium alloy Al5Si deposits in wire and arc additive manufacturing using a cold metal transfer process. *Sci Technol Weld Joining* 23(4):316–332. <https://doi.org/10.1080/13621718.2017.1388995>
25. Almeida P, Williams S (2010) Innovative process model of ti-6al-4v additive layer manufacturing using cold metal transfer (cmt). *Proceedings of the 21st Annual International Solid Freeform Fabrication Symposium*. [S.l.]: [s.n.]
26. Yildiz A, Davut K, Koc B, Yilmaz O (2020) Wire arc additive manufacturing of high-strength low alloy steels: study of process parameters and their influence on the bead geometry and mechanical characteristics. *Int J Adv Manuf Technol* 108:3391–3404. <https://doi.org/10.1007/s00170-020-05482-9>
27. Posch G, Chladil K, Chladil H (2017) Material properties of CMT - metal additive manufactured duplex stainless steel blade-like geometries. *Welding World – Int J Mater Join* 61(5):873–882. <https://doi.org/10.1007/s40194-017-0474-5>
28. ASTM International (2017) E92 - standard test methods for Vickers hardness and Knoop hardness of metallic materials. West Conshohocken
29. Lancaster J (1984) *The Physics of Welding*. Physics in Technology, Northern Ireland
30. Arevalo H, Vilarinho L (2012) Development and assessment of calorimeters using liquid nitrogen and continuous flow (water) for heat input measurement. *Welding Int São Paulo* 17(3):236–250. <https://doi.org/10.1590/S0104-92242012000300008>
31. Xiao Y, Ouden G (1990) A study of GTA weld pool oscillation. *Welding J* 289s–293s

Publisher's Note Springer Nature remains neutral with regard to jurisdictional claims in published maps and institutional affiliations.